Characterizing the Complex Two N#Wave Ionospheric Signature of the 2016 Kaikoura Earthquake

Characterizing the Complex Two N-Wave Ionospheric Signature of the 2016 Kaikoura Earthquake

Justin D. Li,[1] Cody M. Rude,[1,2] Victor Pankratius[1,3]

[1]Data Science in Astro-&Geoinformatics Group, MIT Haystack Observatory, Westford, MA, USA.

[2]Data Science in Astro-&Geoinformatics Group, MIT EAPS, Cambridge, MA, USA.

[3]Data Science in Astro-&Geoinformatics Group, MIT Kavli Institute for Astrophysics and Space Research, Cambridge, MA, USA.

This is the author manuscript accepted for publication and has undergone full peer review but has not been through the copyediting, typesetting, pagination and proofreading process, which may lead to differences between this version and the Version of Record. Please cite this article as doi: 10.1029/2018JA025376

Key Points.

- Developed a statistical approach to detecting the occurrence of TEC disturbances
- Characterized the complex, multiple N-wave shock-acoustic driven CID event
- Suggested a link between the CID complexity and the earthquake's complex structure

Abstract. Major earthquakes (>∼6.5 M_w) can generate observable waves which propagate not only through the Earth but also through the Earth's ionosphere. These traveling ionospheric disturbances can be observed using multi-frequency GPS receivers to measure the ensuing perturbations in the Total Electron Content of the ionosphere. Assisted by a statistical approach we developed to indicate the occurrence of a significant TEC perturbation from the normal background behavior, we detect a traveling ionospheric disturbance generated by the 2016 7.8 M_w Kaikoura earthquake occurring in New Zealand on November 13th. The disturbance was detected ∼8 minutes after the earthquake, propagating towards the equator at ∼1 km/s with a peak-to-peak amplitude of ∼0.22 Total Electron Content units. The coseismic waveform exhibits complex structure unlike that of the expected N-wave for coseismic ionospheric disturbances, with observations of oscillations with 4-minute periodicity and of two N-waves. This observed complexity in the ionosphere likely reflects the impact of the complex, multi-fault structure of the earthquake.

1. Introduction

Ionospheric responses to geophysical events have been documented for a number of sources, such as earthquakes [*Calais and Minster*, 1998; *Heki et al.*, 2006a; *Afraimovich et al.*, 2010; *Liu et al.*, 2010, 2011; *Crowley et al.*, 2016], tsunamis [*Artru et al.*, 2005; *Liu et al.*, 2006; *Tsugawa et al.*, 2011; *Galvan et al.*, 2011, 2012], volcanoes [*Heki*, 2006b; *Shults et al.*, 2016], and storms [*Chou et al.*, 2017]. The Total Electron Content (TEC) of the ionosphere can be measured by multi-frequency GPS receivers at the pierce point between the receiver and the GPS satellite, by comparing the relative phase delays proportionally introduced by the dispersive medium. Ongoing expansion of such GPS networks provides increased capabilities for improved TEC measurements and better monitoring of the ionosphere [*Rolland et al.*, 2011a; *Komjathy et al.*, 2016]. This enables the observation of traveling ionospheric disturbances (TID) generated by such geophysical events and which perturb the ionosphere [*Artru et al.*, 2005] and affect conditions for radio propagation.

Past studies have particularly focused on the 2011 Tohoku earthquake and tsunami [*Liu et al.*, 2011; *Rolland et al.*, 2011b; *Tsugawa et al.*, 2011; *Galvan et al.*, 2012; *Astafyeva et al.*, 2011, 2013; *Crowley et al.*, 2016], with distinct and clearly observed Rayleigh, shock-acoustic, and gravity wave components in the resulting TID. While studies on tsunami-driven TIDs show the resulting oscillatory and extended structure in the perturbations in TEC, events such as volcanoes and earthquakes tend to generate more clearly defined, N-wave shaped TIDs [*Afraimovich et al.*, 2001; *Heki*, 2006b; *Astafyeva et al.*, 2009]. Earthquake driven coseismic ionospheric disturbances (CIDs) are dominated by

Rayleigh and shock acoustic waves, which can be identified by more rapid propagation speeds of ∼3 km/s and ∼1 km/s, as compared to gravity waves generated by tsunamis that propagate at ∼0.3 km/s [*Galvan et al.*, 2012].

The detection of CIDs tends to depend on a >6.5 M_w threshold of the causative earthquake [*Perevalova et al.*, 2014]. Here, we highlight how the 2016 Kaikoura earthquake, with magnitude 7.8, produced a very visible CID observed by the dense GPS network in New Zealand. We clearly detect this CID propagating towards the equator at ∼1 km/s with a ∼0.22 peak-to-peak TECu (TEC unit = 10^{16} el/cm^3) amplitude. The CID shows a strong preferential directionality, with no signal detected traveling poleward, and is visible on GPS satellites with Pseudo Random Noise codes (PRNs) 20, 21, and 29. The form of the observed CID shows a more complex wave pattern rather than the expected single N-wave, suggesting a possible superposition of N-waves from multiple sources. *Hamling et al.* [2017] shows that the Kaikoura earthquake was driven by a complex multi-fault structure that does not fit within the current theoretical and modeling approaches, while recent work points to the likewise more complex ionospheric response with multiple source mechanisms [*Bagiya et al.*, 2018] and source regions [*Lee et al.*, 2018]. This suggests that our observed ionospheric response with two N-waves can support further investigation into the fault structure of the earthquake.

2. Data and Methodology

The Kaikoura earthquake was a significant event of interest in 2016. Relevant information on the measured seismological parameters is available through the United States Geological Survey records (`https://earthquake.usgs.gov/earthquakes/eventpage/us1000778i`). In particular, the earthquake had a magnitude of 7.8 M_w and occurred

at 11:02:56 UTC on November 13 (14th local time), 2016 with an epicenter at 42.757°S, 173.077°E and a depth of 15 km. Surface uplifts of up to 8 m and horizontal offsets of about 6 m were observed, along with a tsunami measuring 3 m in height at Kaikoura [*Hamling et al.*, 2017]. The local time of 00:02:56 NZDT places the event solidly in the nighttime, and magnetospheric conditions were only mildly disturbed with Kp-index, which characterizes the geomagnetic activity, being between 3 and 4- in the preceding and following hours, as shown in Table 1. Aside from several weak flares, there was no significant solar activity during the day of the earthquake event. Similarly, an examination of weather reports shows that no storms or weather activity of any notable strength occurred in this time interval. Thus, any ionospheric activity in this interval is likely to be related to the earthquake itself.

In order to characterize the disturbances in the ionosphere, we obtain TEC measurements and calculate from them differential TEC (dTEC) measurements. Raw GPS data is available in RINEX format through GeoNet - the official source of geological hazard information for New Zealand. After the initial preprocessing of the GPS RINEX data, vertical TEC measurements are available from MIT Haystack Observatory [*Vierinen et al.*, 2016]. These measurements use a set GPS sampling rate of 1 measurement every 30 seconds, and fix the height of the calculated vertical TEC measurement to 350 km. The vertical TEC measurements can then be processed into differential TEC measurements by applying a polynomial fit to estimate the background variations [*Tedd and Morgan*, 1985] or by using a bandpass filter to extract the transient signal of interest [*Savastano et al.*, 2017]. Here, we enforce the constraint that the data is continuous to avoid issues arising from missing

data and fit a 3rd order polynomial. Subtracting the polynomial fit from the original TEC data produces the dTEC measurements used in this study.

The CID signal observed in the TEC and dTEC measurements arises from the coupling between the vertical displacements generated by the earthquake and the atmosphere [*Artru et al.*, 2005]. Although the amplitude of the disturbance is small near the surface, the disturbance is amplified due to the decreasing density of the atmosphere as it propagates upwards. When it reaches the ionosphere, the amplitude is sufficiently large to produce detectable perturbations.

As the earthquake exceeded the 6.5 M_w threshold for producing an ionospheric disturbance [*Perevalova et al.*, 2014], our hypothesis is that a CID should be detectable. We developed and applied a general method for statistically determining whether a CID exists. Using the dTEC measurements from the day before, the day of, and day after the earthquake, we make the assumption that an ionospheric disturbance will result in statistically significant differences in the distribution of the dTEC measurements between the different days. We evaluate this significance by calculating the 2-sample Kolmogorov-Smirnov test, which estimates whether two samples are drawn from different probability distributions, as shown in Figure 1. This example from station 'mahi' and PRN 29 results in a calculated p-value of 0.025, indicating that the observed dTEC behavior differs significantly compared with the surrounding days, when using a significance threshold of $p < 0.05$. From a different visualization, as in the histogram in Figure 1(right), it again becomes readily apparent that the occurrence of a CID alters the distribution of the dTEC measurements.

For the 2016 Kaikoura earthquake, we observe that some 129 GPS station to satellite PRN pairs exhibit a statistically significant difference in dTEC distribution on the day of the earthquake compared to the surrounding days. From that, we conduct further examination through a visual inspection of the dTEC behavior for the identified stations. Here, we observe strong differences between the ionospheric behavior on November 13th and on November 14th. In particular, we observe enhanced wave-like oscillations at the time shortly after the earthquake occurred and which only take place on the day of the earthquake. This holds for multiple stations and several PRN codes (20, 21, and 29). We largely ignore the comparison with the preceding day, November 12th, as the more disturbed geomagnetic conditions result in overall noisier background TEC measurements.

3. Results and Discussion

3.1. CID Characterisics

The strong magnitude of the earthquake and its significant surface displacements resulted in a strong CID. From an examination of the measurements by the array of GPS stations throughout New Zealand paired with GPS satellite PRN 21, we can observe the disturbance propagating radially away from the epicenter of the event. In Figure 2, we present a map of the geographic distribution of GPS stations (white triangles), along with four selected sets of radially directed stations (solid triangles) and the location of their corresponding maximum dTEC measurements (circles with matching colors). The four corresponding inset plots then present the differential TEC time series showing the observed CID, while the peaks across the subplots as plotted on the map reveal the direction of propagation. Of the four example sets of stations and paths, the 'pora' to 'whvr' (cyan) stations path is the weakest. Closer examination of other westward or southward

directed traces do not show any visible disturbances at all. The preference for propagation towards the equator is thus clearly observed [*Heki and Ping*, 2005]. However, further consideration may be required to address possible complicating, non-tectonic effects due to the geomagnetic field and GPS satellite geometry [*Rolland et al.*, 2013; *Bagiya et al.*, 2017].

Similarly, the disturbance can be represented using a hodochron, shown in Figure 3, where the distance for each station's ionospheric pierce point is plotted against the corresponding time with the color indicating the differential amplitude in TECu. We plot hodochrons for satellites with PRNs 20, 21, and 29, which are the three satellites used to observe the event. For reference, the inset plot shows the pierce point paths between these satellites and station 'ahti' to demonstrate the general relative motions of the satellites. The observed form of the CID, as shown by the crests and troughs observed in all three hodochrons, consistently show similar structure and that the disturbance propagates to the ionosphere ∼8 minutes after the earthquake. Observing the potential fits for the propagation velocity of the first crest, we find that the speed is ∼1 km/s. This estimated velocity confirms that this TID is a coseismic event, and in particular, that it is driven by the shock acoustic mechanism [*Afraimovich et al.*, 2001]. Furthermore, our examination of the southward component of the hodochrons again confirms that the CID does not noticeably propagate poleward.

3.2. CID Complexity

The form of the disturbance observed in the hodochron, as well as in the time series plots, shows a more complex structure for the CID than otherwise expected. Typical earthquake induced disturbances, which propagate as Rayleigh or shock-acoustic waves,

tend to exhibit an N-wave appearance [*Afraimovich et al.*, 2001; *Astafyeva et al.*, 2009]. Here though, we observe a rather more complex profile for the CID, with multiple oscillations that occur for an extended duration. In fact, such a waveform more closely resembles the gravity waves produced by a tsunami and which propagate along the tsunami wave fronts [*Rolland et al.*, 2011b; *Galvan et al.*, 2012]. As the characteristics of this event, primarily the estimated propagation time and velocity, indicate that this TID is clearly a coseismic event, we instead attribute this unexpected and unusually complex structure of the CID to the characteristics of the originating earthquake.

While CIDs with complex profiles have been noted before, the complexity is typically introduced by waves originating from the different types of source mechanisms. For example, the observed complexity and duration of the ionospheric disturbance in the 2011 Tohoku earthquake is driven not only by the Rayleigh and shock-acoustic waves resulting from the earthquake, but also by the gravity wave components induced by the tsunami [*Liu et al.*, 2011; *Rolland et al.*, 2011b; *Galvan et al.*, 2012]. Even in the examples where the CID component exhibits greater complexity than the theoretical N-wave profile, the additional complexity tends to behave more as enhanced noise or oscillatory perturbations [*Astafyeva et al.*, 2011; *Choosakul et al.*, 2009] rather the structured superposition of additional N-wave components observed here.

This complexity is observed in the dTEC measurements for all three of these satellites and is at its strongest in three different GPS stations, 'birf' with PRN 20, 'hikb' with PRN 21, and 'bthl' with PRN 29, as shown in Figure 4. The time series representations in the left column show how the dTEC signal oscillates multiple times, rather than clearly exhibiting one or two N-waves. Stations 'birf' and 'hikb' show that the oscillations are of

significant strength, falling off approximately exponentially, and of significant duration, lasting ∼30 minutes from the start of the disturbance. These oscillations, as measured for 'hikb', exhibit a periodicity of 4-minutes. This periodicity is similar to that observed as resulting from the 2015 volcanic eruption at Calbuco, in Chile [*Aoyama et al.*, 2016], and from the Sumatra-Andaman earthquake in 2004 [*Choosakul et al.*, 2009]. However, the occurrence of these oscillations immediately following the earthquake, distinguishes them from the induced long-lasting oscillations occurring over an hour later [*Choosakul et al.*, 2009] and instead resemble those produced from the atmospheric gravity waves generated by the source event [*Aoyama et al.*, 2016]. Furthermore, by fitting propagation velocities to the crests and troughs in the hodochrons, on the right, we find that all of the velocities fall between 1 km/s and 1.5 km/s, as presented in Table 2. This indicates that the waves are all predominantly shock-acoustic in origin throughout this interval. A closer examination of the CID suggests that this observed complexity is due to the more complex structure of the Kaikoura earthquake.

Unlike the normal behavior described by the standard theoretical approach and modeling of earthquakes, the behavior of the Kaikoura earthquake demonstrated unexpected ruptures along numerous faults with diverse orientations [*Hamling et al.*, 2017]. Not only are the observed surface displacements spread out rather than concentrated at a single epicenter, but the modeled sources for the ionospheric disturbances are likewise not centered at a single epicenter for the earthquake [*Lee et al.*, 2018]. As a result, we suggest that the observed CID could be considered as a superposition of multiple shock-acoustic induced waves. This is supported by the measurements made between 'bthl' and PRN 29, shown in Figure 4, where at least two distinct wave packets are observed appearing as

two consecutive N-waves. In fact, the overall hodochron for PRN 29 appears to exhibit these two N-waves, as marked by the two black arrows in the lower panel of Figure 4. We can look at other station-PRN pairs in the same manner and examine in Figure 5 the dTEC measurements between PRN 29 and stations 'otak', 'levn', 'rdlv', and 'cmbl', in addition to 'bthl'. Although the stations do not all show the behavior as clearly as for 'bthl', the occurrence of two separate packets of N-waves can still be distinguished for each station. In order to identify where these two N-waves occurred, we also plot the geographic pierce point locations for the central peak for each packet, with a circle and square symbol respectively, on the map in Figure 5. The marker colors also match with the corresponding GPS station label, highlighted by the colored box. The timing of these two packets within this half hour interval (the separation delay ranges between 15 minutes and 20 minutes), and the lack of any other sufficiently strong event in the region, suggests that the greater complexity in the underlying structure of the faults for the Kaikoura earthquake is reflected in the ionospheric response. The surface ruptures, marked on the map in thick red lines, come from the observations by *Hamling et al.* [2017] and show the relative position of the source regions relative to the measurement locations. The spatial orientation of the occurrence of the CID complexity aligns well with the orientation of the surface displacements, which occurred along the multiple sub-faults. Similarly, we observe that the strongest propagation of this complex wave structure along the 'cnst' to 'hikb' path in Figure 2 likewise aligns with the same orientation of the multi-fault rupture structure of the earthquake. With our observations, along with modeling work focusing on two possible source regions [*Bagiya et al.*, 2018; *Lee et al.*, 2018], we tentatively link

the earthquake's unusually complex rupture structure with at least two fault regions as the source for the more complex CID.

The possibility of this superposition of CIDs driven by multiple rupturing faults aligns well with the observation of a possible two segment TEC perturbation observed in the 2011 Tohoku earthquake [*Astafyeva et al.*, 2013]. Using more sensitive, 1 Hz GPS measurements, *Astafyeva et al.* [2013] noted the occurrence of two separate focal regions and TEC enhancements which later merge together. Similarly, *Heki et al.* [2006a] observed multiple peaks in the CID for the 2004 Sumatra earthquake, which they modeled as resulting from CIDs generated by distinct segments of that earthquake. Here, we extend this idea of CID superposition resulting from multiple segments rupturing along a single fault to the 2016 Kaikoura earthquake and the possible superposition resulting from multiple sub-faults ruptures. The complexity is also supported by the observation of the two distinct N-wave packets, which differs from other complexity such as more oscillatory behavior resulting from acoustic resonance [*Choosakul et al.*, 2009].

Recent work by *Bagiya et al.* [2018] also examines the ionospheric perturbations resulting from the 2016 Kaikoura earthquake. Their dTEC observations and measurements are in good agreement with our results and likewise identify the complex tectonics driving this event. However, their focus is on explaining the orientation of their observation of a single N-wave, which is detected in an unusual distribution around the source region. In particular, they focus on the displacements at 'cmbl' and 'kaik' and use modeling to estimate that two source regions, at the Campbell and Kaikoura Coseismic Thrust Zones, are responsible for the directionality of their observations. Here, we focus in greater detail on the dTEC observations and are guided by our statistical approach to detecting significant

ionospheric perturbations. As a result, we do not find the station to PRN 5 signals to be as statistically significant as our observations using PRN 29. Moreover, for a number of these stations, as shown in Figure 5, we observe two disturbances, appearing to be two distorted N-waves, generated by the earthquake event. Combined with the modeling work on the tectonic thrust zones [*Bagiya et al.*, 2018], we hypothesize that there is still greater complexity in this region and that there are at least two source regions associated with the multi-fault rupture structure of the 2016 Kaikoura earthquake.

Another recent work examining the complexities of the Kaikoura earthquake, by *Lee et al.* [2018], applies backpropagation modeling to identify a shifted source location for the ionospheric disturbance as compared with the recorded earthquake's epicenter. Again, their observations of the CID and estimates on the propagation speed are in good agreement with our results. They further note the possibility of multiple source regions, due to the incomplete fit of the observed hodochrons with their modeling of a single source location. Interestingly, part of their challenge in accurately modeling the disturbance is attributed to additional complexity, with a distorted N-wave shape and the suggestions of a secondary N-shaped wave. Our work provides more support for this additional complexity, through our clearer observations of two N-waves. However, it is likely that further modeling and analysis is needed, as the separation in timing between the two N-wave packets is not insignificant. In particular, the estimated duration of the earthquake, from examining the moment rate over time, is 2 minutes. This fits well with the work by *Lee et al.* [2018], who compared two epicenters separated by $\sim$ 1 minute for their modeling. However, the two N-waves in our observation are separated by $\sim$ 15 or $\sim$ 20 minutes, depending on the exact station. Consequently, we can only tentatively link the

CID complexity to the Kaikoura earthquake based on our empirical observations, leaving space for further work to explore possible mechanisms or alternate sources. We observe that the second N-wave disturbance is quite distinct, exhibiting similar magnitude and profile characteristics to the first N-wave. Significantly, no other causal source activity is observed within this duration, and the aftershocks occurring within the following 20 minutes are all significantly weaker, with magnitude $<6.0 M_W$, which would not be expected to independently generate any ionospheric signature.

4. Conclusion

Our report here of our characterization of the CID generated from the 2016 Kaikoura earthquake provides a statistical approach for assisting in the detection of ionospheric disturbances and highlights some unusual complexity resulting from the more complex tectonics governing this earthquake. While the observations as a whole fit well with observations of TIDs from other high magnitude earthquakes and with the recent work on the Kaikoura earthquake [*Bagiya et al.*, 2018; *Lee et al.*, 2018], instead of the typical single N-wave structure of the CID, we note the occurrence of two N-waves and additional 4-minute oscillations shortly after the time of the earthquake in the dTEC waveforms. These observations suggest the influence of multiple source regions, driven by the multi-fault structure of this unusually complex earthquake. Detection of similar such complexity for other earthquakes may lead to greater understanding for mapping the behavior between displacements and the ionospheric response, while a comparison with any similar complexity resulting from other types of source events may likewise provide insight into improving our understanding of the mechanisms governing the behavior of that type of source event as well.

Acknowledgments. We acknowledge support for this work from NASA AIST NNX15AG84G, NSF ACI-1442997, NSF AGS-1343967, and NSF AGS-1242204. This research was mainly conducted while the authors were with MIT Haystack Observatory. We thank Olusegun F. Jonah, Michael G. Gowanlock, and Guillaume Rongier for their helpful discussions and editing. The GPS data is produced by GeoNet - the official source of geological hazard information for New Zealand, and the TEC data is available through the World-wide GPS Receiver Network data product from Massachusetts Institute of Technology Haystack Observatory, which can be accessed through http://cedar.openmadrigal.org/. We thank Anthea J. Coster and William Rideout for their assistance in obtaining and processing the TEC and dTEC data. Kp index data can be accessed from wdc.kugi.kyoto-u.ac.jp/kp, and data for solar and geophysical events can be accessed from ftp://ftp.swpc.noaa.gov/pub/indices/events/.

References

Aoyama, T., T. Iyemori, K. Nakanishi, M. Nishioka, D. Rosales, O. Veliz, and E. V. Safor (2016), Localized field-aligned currents and 4-min TEC and ground magnetic oscillations during the 2015 eruption of Chile's Calbuco volcano, *Earth Planet Sp*, *68*(148), doi: 10.1186/s40623-016-0523-0.

Afraimovich, E. L., N. P. Perevalova, A. V. Plotnikov, and A. M. Uralov (2001), The shock-acoustic waves generated by earthquakes, *Annales Geophysicae*, *19*(4), 395–409, doi:10.5194/angeo-19-395-2001.

Afraimovich, E. L., D. Feng, V. V. Kiryushkin, and E. I. Astafyeva (2010), Near-field TEC response to the main shock of the 2008 Wenchuan earthquake, *Earth, Planets and*

Space, *62*(11), 899–904, doi:10.5047/eps.2009.07.002.

Artru, J., V. Ducic, H. Kanamori, P. Lognonné, and M. Murakami (2005), Ionospheric detection of gravity waves induced by tsunamis, *Geophysical Journal International*, *160*(3), 840–848, doi:https://doi.org/10.1111/j.1365-246X.2005.02552.x.

Astafyeva, E., K. Heki, V. Kiryushkin, E. Afraimovich, and S. Shalimov (2009), Two-mode long-distance propagation of coseismic ionosphere disturbances, *Journal of Geophysical Research: Space Physics*, *114*(A10), doi:10.1029/2008JA013853.

Astafyeva, E., P. Lognonné, and L. Rolland (2011), First ionospheric images of the seismic fault slip on the example of the Tohoku-oki earthquake, *Geophysical Research Letters*, *38*(L22104), doi:10.1029/2011GL049623.

Astafyeva, E., L. Rolland, P. Lognonné, K. Khelfi, and T. Yahagi (2013), Parameters of seismic source as deduced from 1Hz ionospheric GPS data: Case study of the 2011 Tohoku-oki event, *Journal of Geophysical Research: Space Physics*, *118*(59425950), doi: 10.1002/jgra.50556.

Bagiya, M. S., A. S. Sunil, P. S. Sunil, K. M. Sreejith, L. Rolland, and D. S. Ramesh (2017), Efficiency of coseismic ionospheric perturbations in identifying crustal deformation pattern: Case study based on M_w 7.3 May Nepal 2015 earthquake, *Journal of Geophysical Research: Space Physics*, *122*(A6849-6857), doi:10.1002/2017JA024050.

Bagiya, M. S., P. S. Sunil, A. S. Sunil, and D. S. Ramesh (2018), Coseismic Contortion and Coupled Nocturnal Ionospheric Perturbations During 2016 Kaikoura, M_w 7.8 New Zealand earthquake, *Journal of Geophysical Research: Space Physics*, *123*(1477-1487), doi:10.1002/2017JA024584.

Calais, E., and J. B. Minster (1998), GPS, earthquakes, the ionosphere, and the Space Shuttle, *Physics of the Earth and Planetary Interiors*, *105*(3), 167 – 181, doi:10.1016/S0031-9201(97)00089-7.

Choosakul, N., A. Saito, T. Iyemori, and M. Hashizume (2009), Excitation of 4-min periodic ionospheric variations following the great Sumatra-Andaman earthquake in 2004, *Journal of Geophysical Research: Space Physics*, *114*(A10313), doi:10.1029/2008JA013915.

Chou, M. Y., C. C. H. Lin, J. Yue, H. F. Tsai, Y. Y. Sun, J. Y. Liu, and C. H. Chen (2017), Concentric traveling ionosphere disturbances triggered by Super Typhoon Meranti (2016), *Geophysical Research Letters*, *44*(3), 1219–1226, doi:10.1002/2016GL072205.

Crowley, G., I. Azeem, A. Reynolds, T. M. Duly, P. McBride, C. Winkler, and D. Hunton (2016), Analysis of traveling ionospheric disturbances (TIDs) in GPS TEC launched by the 2011 Tohoku earthquake, *Radio Science*, *51*(5), 507–514, doi:10.1002/2015RS005907.

Galvan, D. A., A. Komjathy, M. P. Hickey, and A. J. Mannucci (2011), The 2009 Samoa and 2010 Chile tsunamis as observed in the ionosphere using GPS total electron content, *Journal of Geophysical Research: Space Physics*, *116*(A6), doi:10.1029/2010JA016204.

Galvan, D. A., A. Komjathy, M. P. Hickey, P. Stephens, J. Snively, Y. T. Song, M. D. Butala, and A. J. Mannucci (2012), Ionospheric signatures of Tohoku-Oki tsunami of March 11, 2011: Model comparisons near the epicenter, *Radio Science*, *47*(4), doi:10.1029/2012RS005023.

Hamling, I. J., S. Hreinsdóttir, K. Clark, J. Elliott, C. Liang, E. Fielding, N. Litchfield, P. Villamor, L. Wallace, T. J. Wright, E. D'Anastasio, S. Bannister, D. Bur-

bidge, P. Denys, P. Gentle, J. Howarth, C. Mueller, N. Palmer, C. Pearson, W. Power, P. Barnes, D. J. A. Barrell, R. Van Dissen, R. Langridge, T. Little, A. Nicol, J. Pettinga, J. Rowland, and M. Stirling (2017), Complex multifault rupture during the 2016 M_w 7.8 Kaikōura earthquake, New Zealand, *Science*, doi:10.1126/science.aam7194.

Heki, K., and J. Ping (2005), Directivity and apparent velocity of the coseismic ionospheric disturbances observed with a dense GPS array, *Earth and Planetary Science Letters*, *236*(3), 845 – 855, doi:10.1016/j.epsl.2005.06.010.

Heki, K., Y. Otsuka, N. Choosakul, N. Hemmakorn, T. Komolmis, and T. Maruyama (2006a), Detection of ruptures of Andaman fault segments in the 2004 great Sumatra earthquake with coseismic ionospheric disturbances, *Journal of Geophysical Research: Solid Earth*, *111*(B9), doi:10.1029/2005JB004202.

Heki, K. (2006b), Explosion energy of the 2004 eruption of the Asama Volcano, central Japan, inferred from ionospheric disturbances, *Geophysical Research Letters*, *33*(14), doi:10.1029/2006GL026249.

Komjathy, A., Y. M. Yang, X. Meng, O. Verkhoglyadova, A. J. Mannucci, and R. B. Langley (2016), Review and perspectives: Understanding natural-hazards-generated ionospheric perturbations using GPS measurements and coupled modeling, *Radio Science*, *51*(7), 951–961, doi:10.1002/2015RS005910.

Lee, R. F., L. M. Rolland, and T. D. Mikesell (2018), Seismo-Ionospheric Observations, Modeling, and Backprojection of the 2016 Kaikōura Earthquake, *Bulletin of the Seismological Society of America*, *108*(3B), 1794-1806, doi:10.1785/0120170299.

Liu, J. Y., Y. B. Tsai, K. F. Ma, Y. I. Chen, H. F. Tsai, C. H. Lin, M. Kamogawa, and C. P. Lee (2006), Ionospheric GPS total electron content (TEC) disturbances triggered

by the 26 December 2004 Indian Ocean tsunami, *Journal of Geophysical Research: Space Physics*, *111*(A5), doi:10.1029/2005JA011200.

Liu, J. Y., H. F. Tsai, C. H. Lin, M. Kamogawa, Y. I. Chen, C. H. Lin, B. S. Huang, S. B. Yu, and Y. H. Yeh (2010), Coseismic ionospheric disturbances triggered by the Chi-Chi earthquake, *Journal of Geophysical Research: Space Physics*, *115*(A8), doi: 10.1029/2009JA014943.

Liu, J. Y., C. H. Chen, C. H. Lin, H. F. Tsai, C. H. Chen, and M. Kamogawa (2011), Ionospheric disturbances triggered by the 11 March 2011 $M9.0$ Tohoku earthquake, *Journal of Geophysical Research: Space Physics*, *116*(A6), doi:10.1029/2011JA016761.

Perevalova, N., V. Sankov, E. Astafyeva, and A. S. Zhupityaeva (2014), Threshold magnitude for Ionospheric TEC response to earthquakes, *Journal of Atmospheric and Solar-Terrestrial Physics*, *108*(Supplement C), 77 – 90, doi:10.1016/j.jastp.2013.12.014.

Rolland, L. M., P. Lognonné, and H. Munekane (2011a), Detection and modeling of Rayleigh wave induced patterns in the ionosphere, *Journal of Geophysical Research: Space Physics*, *116*(A5), doi:10.1029/2010JA016060.

Rolland, L. M., P. Lognonné, E. Astafyeva, E. A. Kherani, N. Kobayashi, M. Mann, and H. Munekane (2011b), The resonant response of the ionosphere imaged after the 2011 off the Pacific coast of Tohoku Earthquake, *Earth, Planets and Space*, *63*(7), doi:10.5047/eps.2011.06.020.

Rolland, L. M., M. Vergnolle, J. M. Nocquet, A. Sladen, J. X. Dessa, F. Tavakoli, H. R. Nankali, and F. Cappa (2013), Discriminating the tectonic and non-tectonic contributions in the ionospheric signature of the 2011, $M_w7.1$, dip-slip Van earthquake, Eastern Turkey, *Geophysical Research Letters*, *40*(25182522), doi:10.1002/grl.50544.

Savastano, G., A. Komjathy, O. Verkhoglyadova, A. Mazzoni, M. Crespi, Y. Wei, and A. J. Mannucci (2017), Real-Time Detection of Tsunami Ionospheric Disturbances with a Stand-Alone GNSS Receiver: A Preliminary Feasibility Demonstration, *Scientific Reports*, *7*, doi:10.1038/srep46607.

Shults, K., E. Astafyeva, and S. Adourian (2016), Ionospheric detection and localization of volcano eruptions on the example of the April 2015 Calbuco events, *Journal of Geophysical Research: Space Physics*, *121*(10), 10,303–10,315, doi:10.1002/2016JA023382.

Tedd, B. L., and M. G. Morgan (1985), TID observations at spaced geographic locations, *Journal of Geophysical Research: Space Physics*, *90*(A12), 12,307–12,319, doi:10.1029/JA090iA12p12307.

Tsugawa, T., A. Saito, Y. Otsuka, M. Nishioka, T. Maruyama, H. Kato, T. Nagatsuma, and K. T. Murata (2011), Ionospheric disturbances detected by GPS total electron content observation after the 2011 off the Pacific coast of Tohoku earthquake, *Earth, Planets and Space*, *63*(7), 66, doi:10.5047/eps.2011.06.035.

Vierinen, J., A. J. Coster, W. C. Rideout, P. J. Erickson, and J. Norberg (2016), Statistical framework for estimating GNSS bias, *Atmospheric Measurement Techniques*, *9*(3), 1303–1312, doi:10.5194/amt-9-1303-2016.

Date	**3-Hour Interval Kp values**							
11/12/2016	3-	4-	2+	4	4-	3+	3	3+
11/13/2016	4-	4-	3+	*3+*	3	3	5-	4-
11/14/2016	1+	2+	2+	2+	3-	3	2-	3

Table 1. The 3-hour Kp values, characterizing the geomagnetic activity, for the time interval around the Kaikoura earthquake, from 11/12/2016 to 11/14/2016. The earthquake occurred at 11:02:56 UTC, which falls in the 9-12 UTC bin (the fourth Kp column), and has a Kp of 3+, which has been italicized.

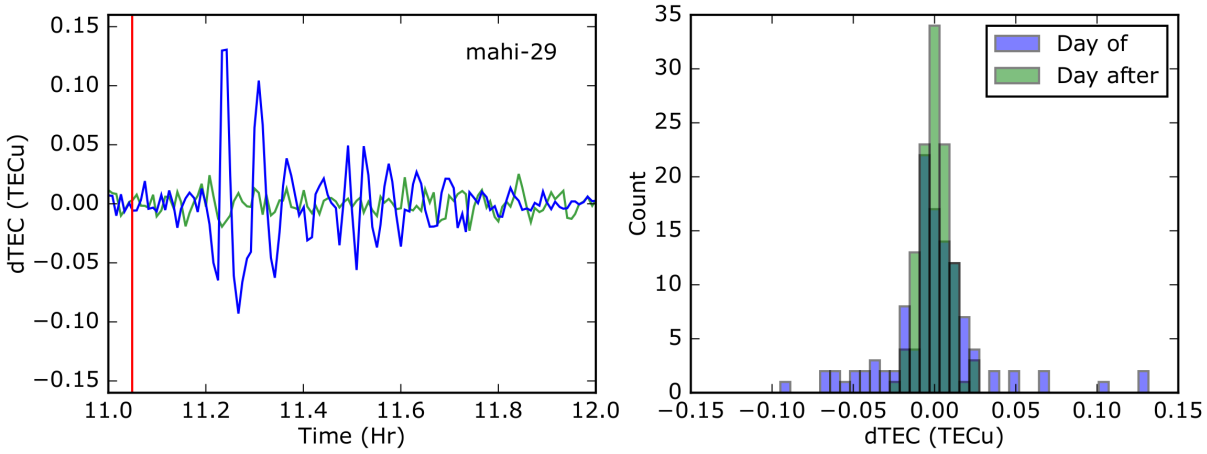

Figure 1. Example dTEC measurement (left) from station 'mahi' and PRN 29, showing the difference in distribution (right) between the day of the event (blue) and the following day (green). The calculated Kolmogorov-Smirnov p-value, here $p = 0.025$, indicates that the sample dTEC values are drawn from different distributions. For reference, the vertical red line indicates the time of the earthquake.

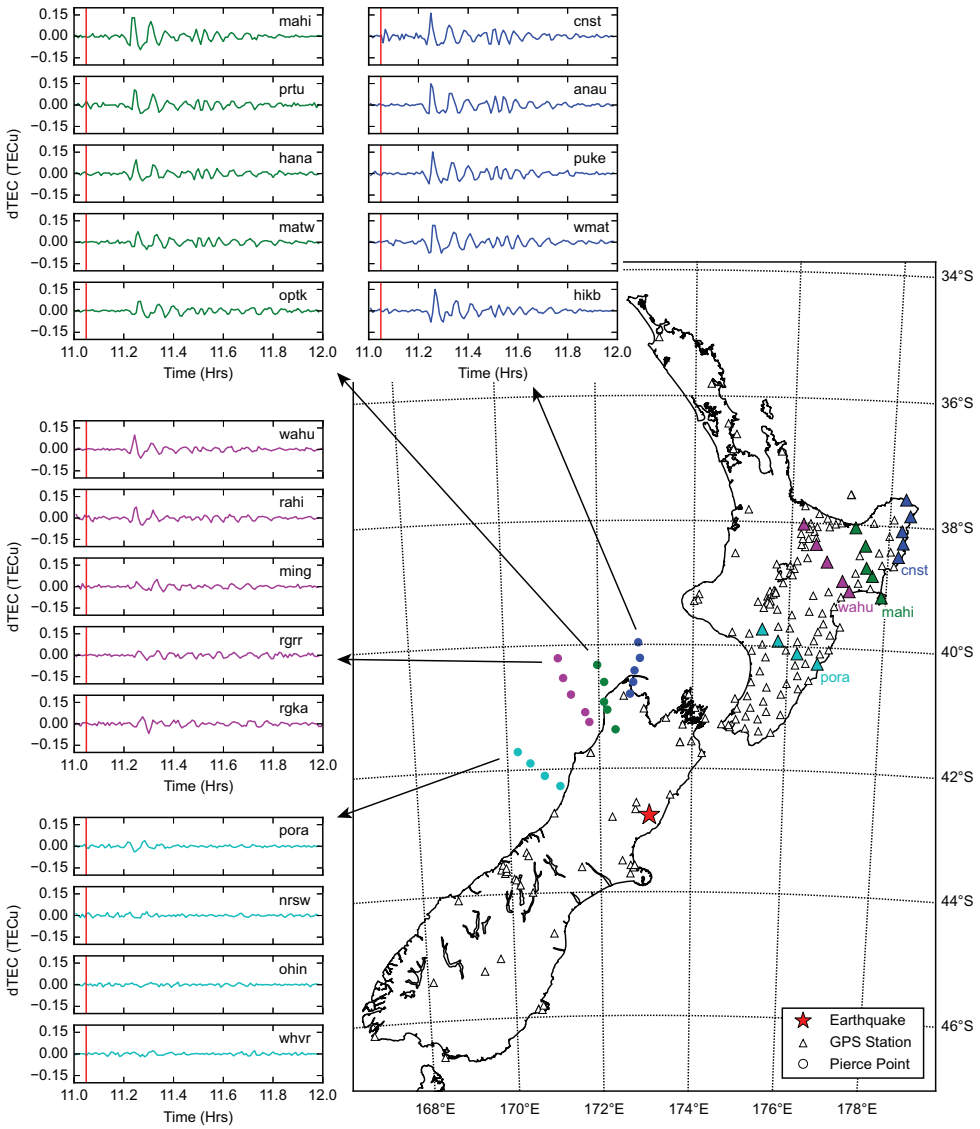

Figure 2. Map of the Kaikoura earthquake region illustrating the radial propagation of the traveling ionospheric disturbance at selected pierce point observations, at a height of 350 km. The regions dense GPS station network is indicated by the triangle markers, while a subset of filled triangles are paired by color with circular markers indicting the maximum ionospheric pierce point locations for GPS satellite PRN 21. The marker colors (blue, green, magenta, and cyan) correspond to the inset subplots of the differential TEC measurements. The vertical red line in the subplots marks the time of the earthquake, and each station name is included in the upper right for reference.

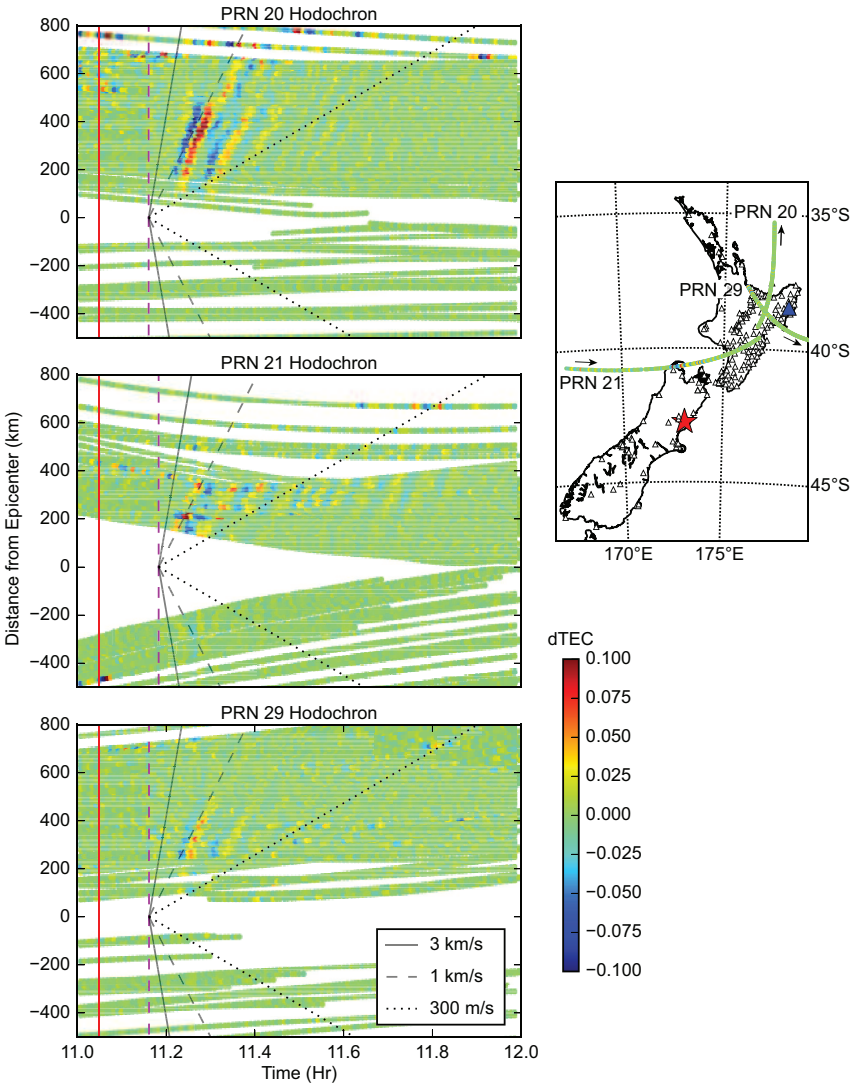

Figure 3. Hodochron observations of the coseismic ionospheric disturbance using three GPS satellites. The paths of the ionospheric piece points between the three satellites, with their corresponding PRN code and direction of motion, and station 'ahti' (the blue triangle) are shown in the inset map. The hodochrons show the changes in dTEC (units in TECu) according to the color scale as a function of the time on the x-axis and the distance from the epicenter of the earthquake on the y-axis (North being positive, and South negative). The vertical red line in the hodochron subplots marks the time of the earthquake, while the dashed vertical magenta line estimates the time at which the CID reaches the ionosphere. The three black lines (solid, dashed, and dotted) show the propagation speeds of 3 km/s, 1 km/s, and 300 m/s respectively.

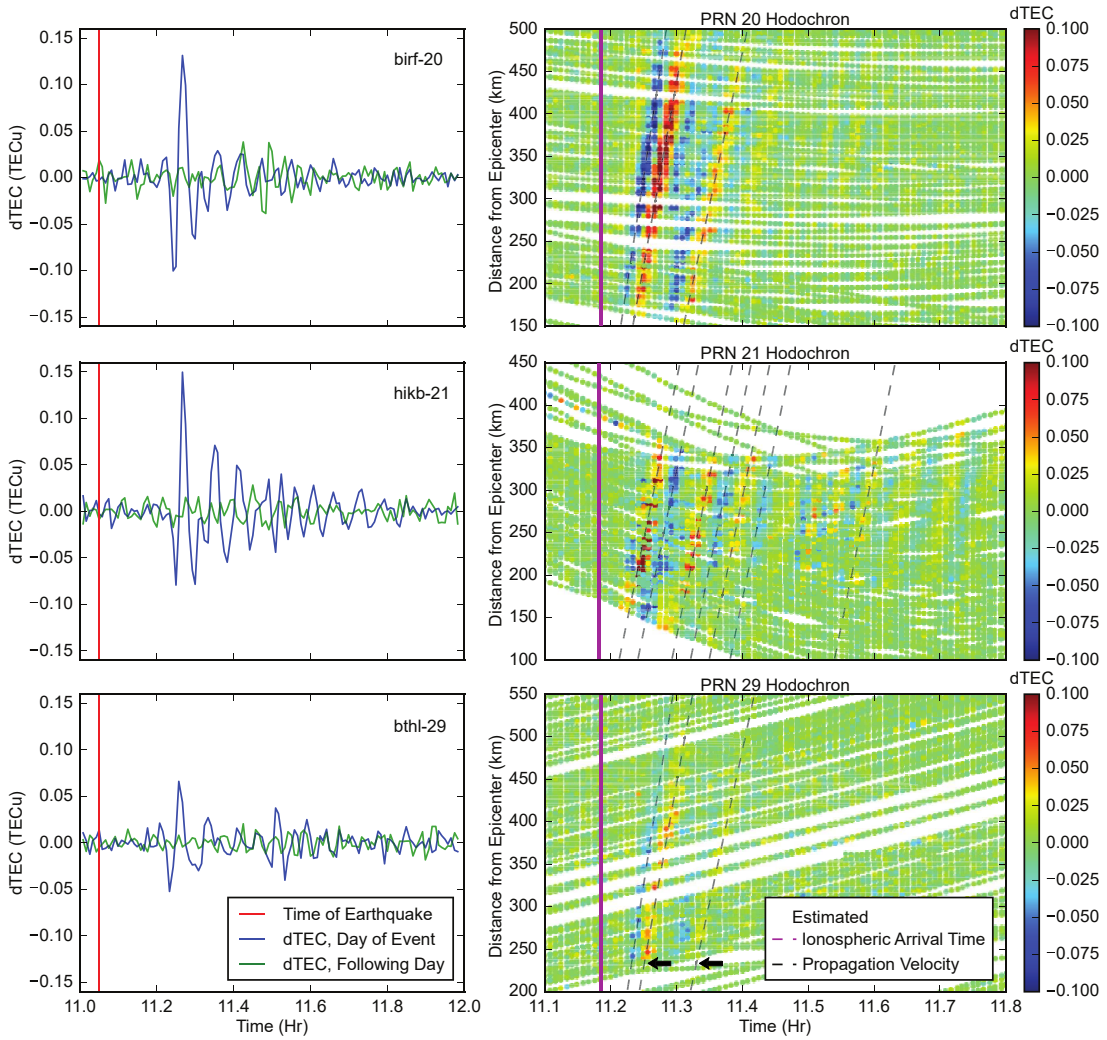

Figure 4. Close up examination of the observed complexity in the dTEC time series and in the hodochron observations. The maximum peak amplitude dTEC time series for each GPS station and satellite PRN pair is shown on the left. The vertical red line denotes the time of the earthquake, while the dTEC is shown for the day of the event (blue) and for the following day (green). The inset text describes the GPS station and the satellite PRN. The corresponding hodochron for a given satellite is shown on the right, with the vertical magenta line showing the time of arrival of the CID at the ionosphere. Dashed black lines mark the estimated propagation velocities over multiple crests and troughs for each PRN, and the 2 black arrows in the PRN 29 hodochron indicates the two separate N-waves.

Satellite	**Propagation velocity fits, from left to right**						
PRN 20	1.4 km/s	1.2 km/s	1 km/s				
PRN 21	1.05 km/s	1.05 km/s	1.05 km/s	1.05 km/s	1.05 km/s	1.05 km/s	1.05 km/s
PRN 29	1.4 km/s	1.2 km/s	1 km/s				

Table 2. Slopes characterizing the fitted propagation velocities of the CID crests and troughs for the hodochrons for satellites 20, 21, and 29 from Figure 3.

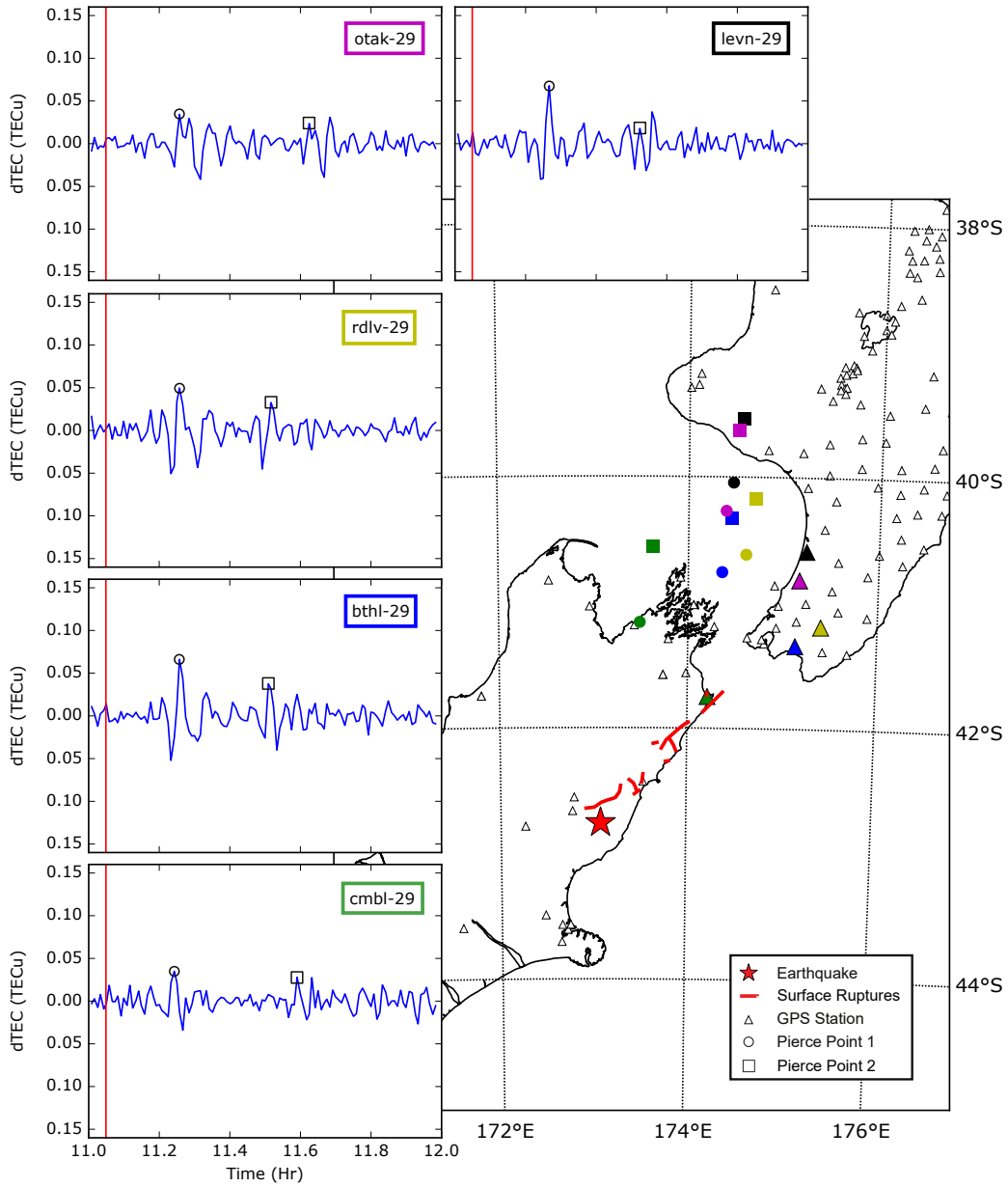

Figure 5. Examples highlighting the observed complexity in the ionospheric response to the Kaikoura earthquake with inset plots of dTEC measurements at five GPS stations. The vertical red line marks the time of the earthquake, and each station name is included in the upper right for reference with the corresponding colors for the station and pierce point locations on the map. The circular marker and the square marker are included to distinguish the location and timing for the two peaks of the distinct N-waves. The map is focused in on a closer region around Kaikoura and shares the same labeling as in Figure 2, with the addition of the surface ruptures observed by Hamling marked on the map in red.

Figure 1.

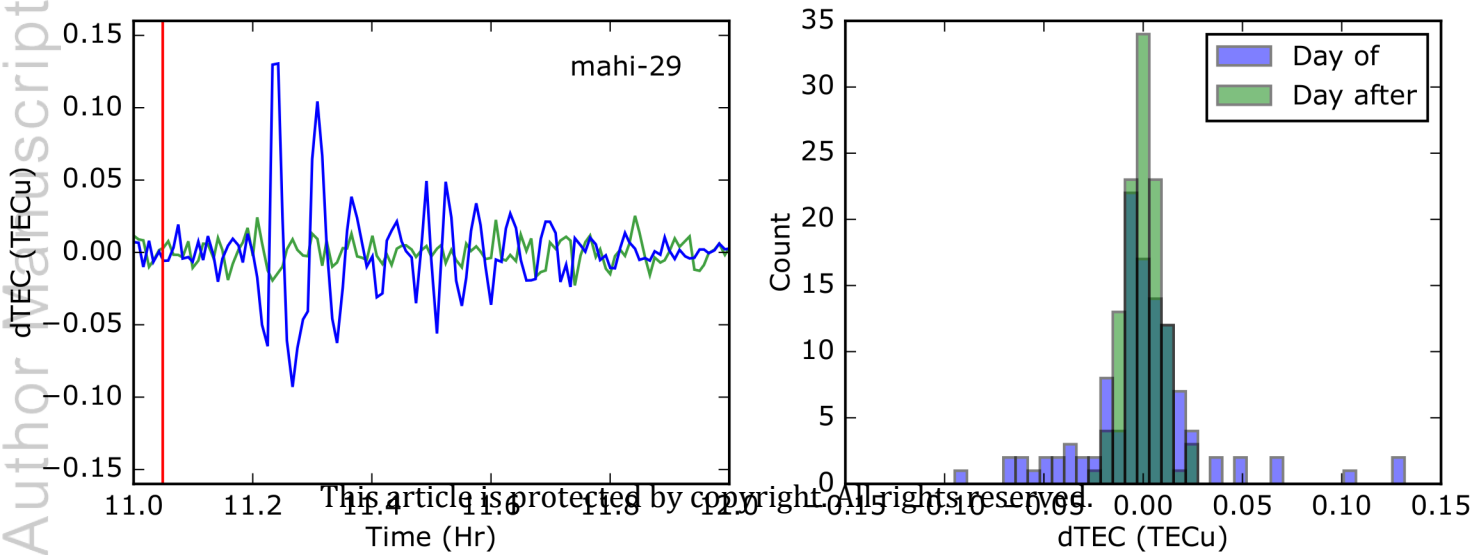

Figure 2.

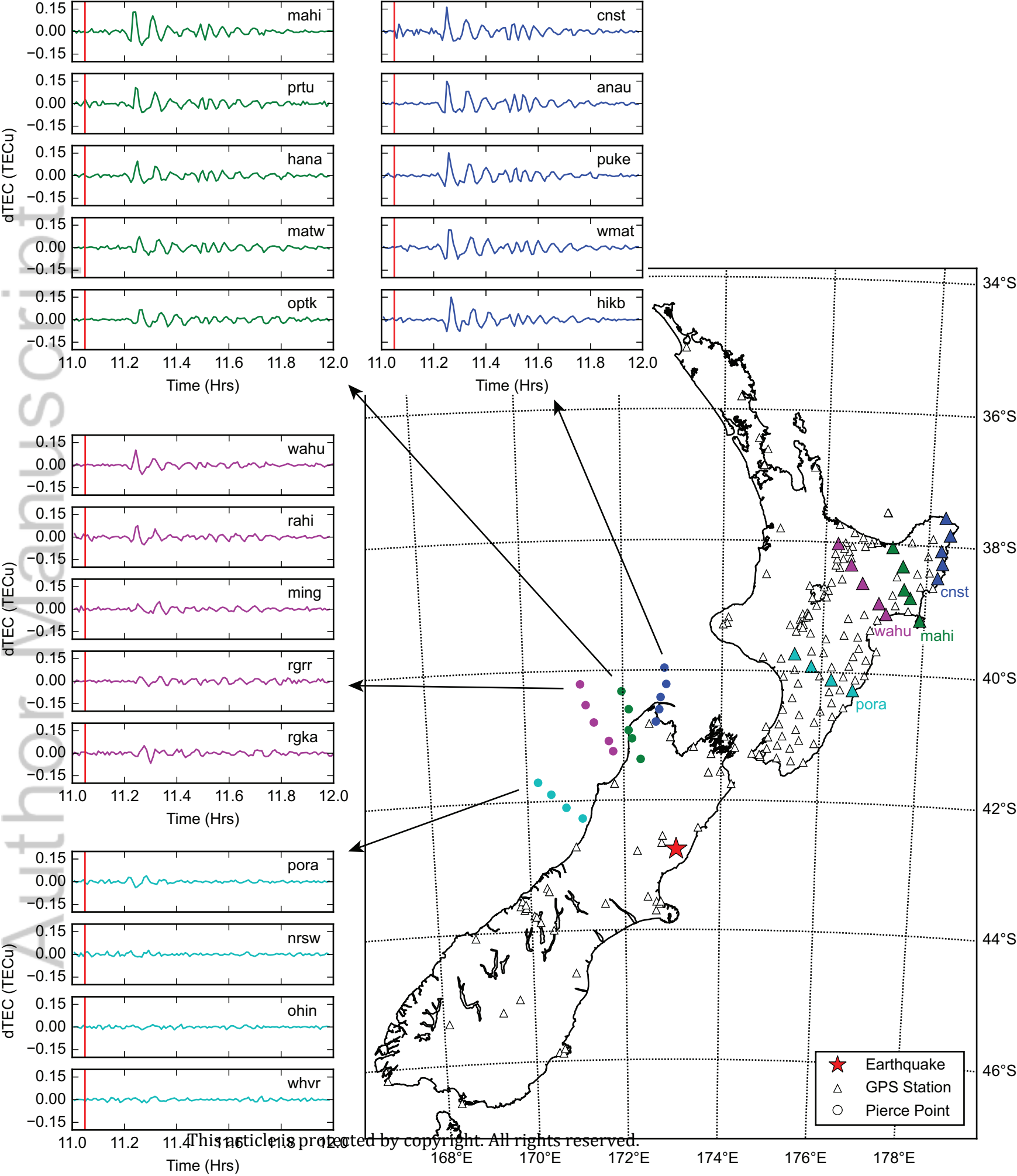

Figure 3.

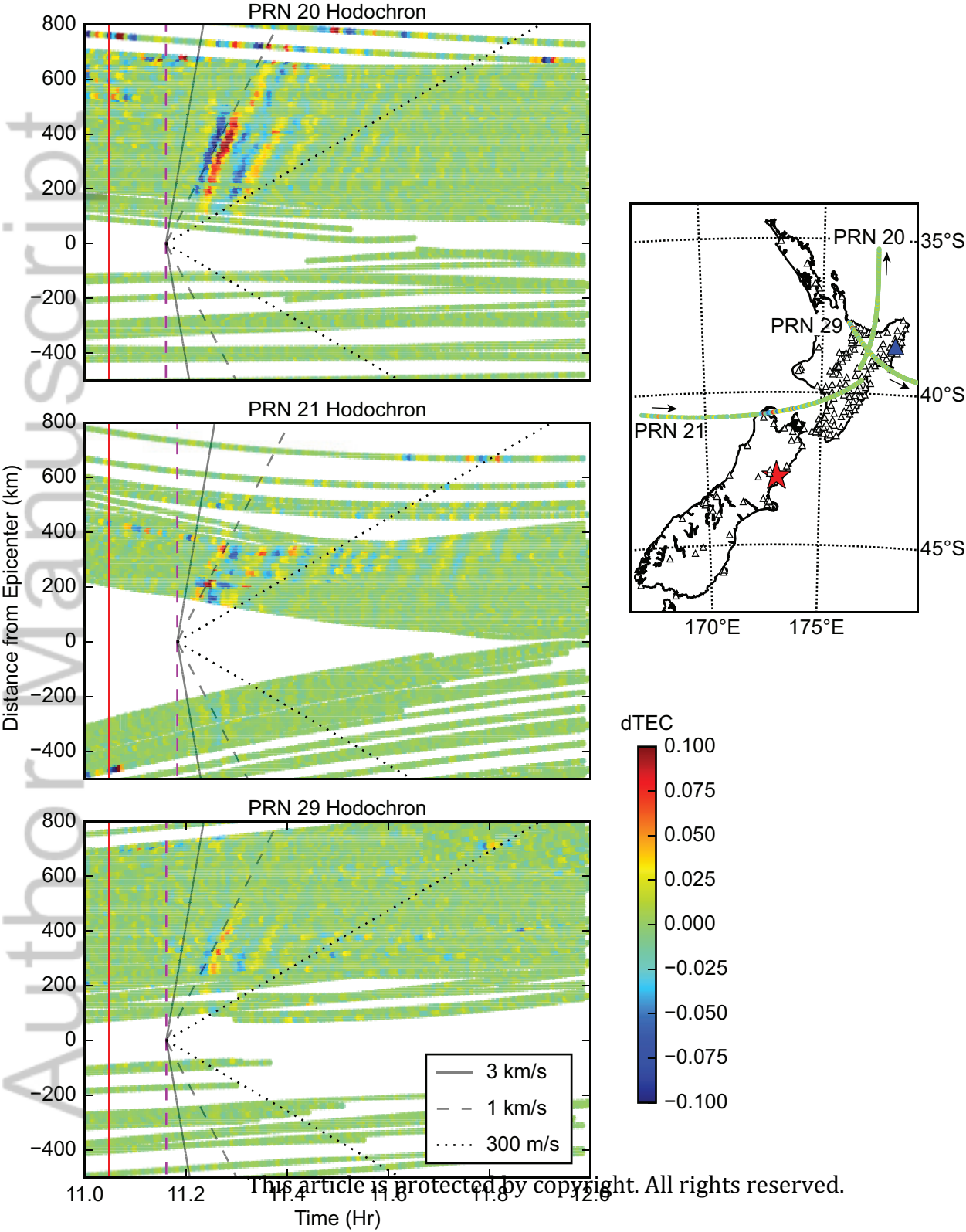

Figure 4.

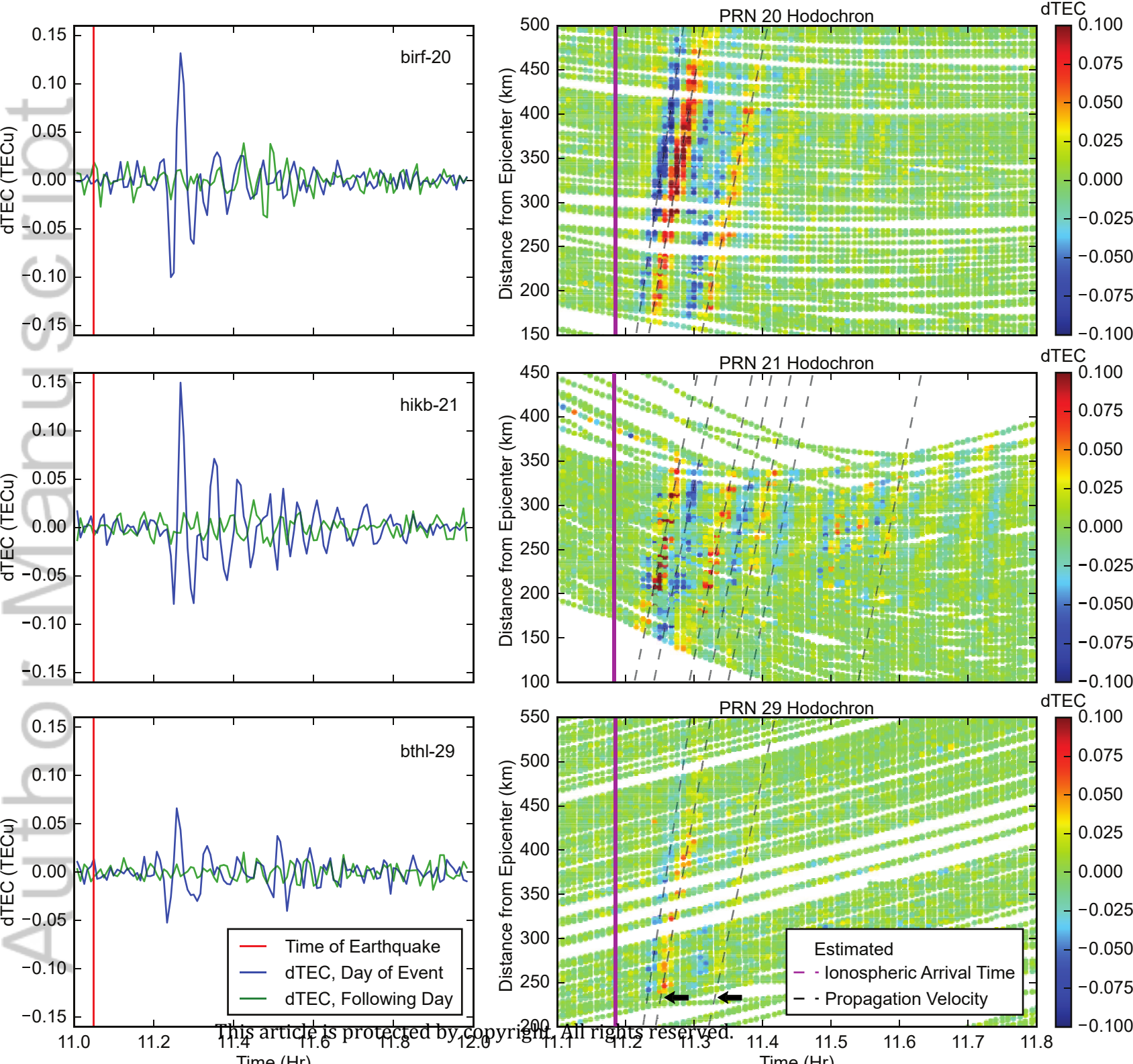

Figure 5.

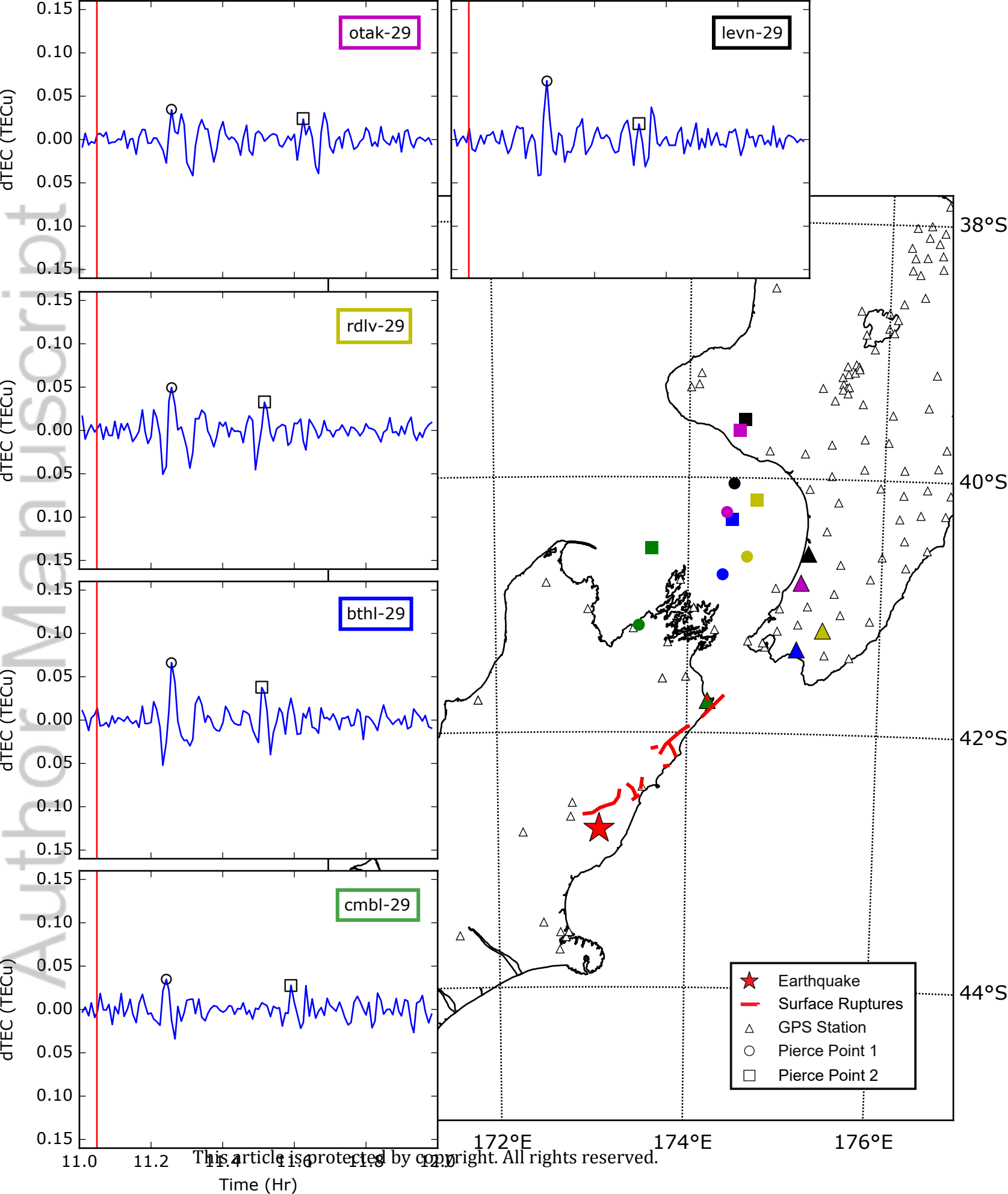

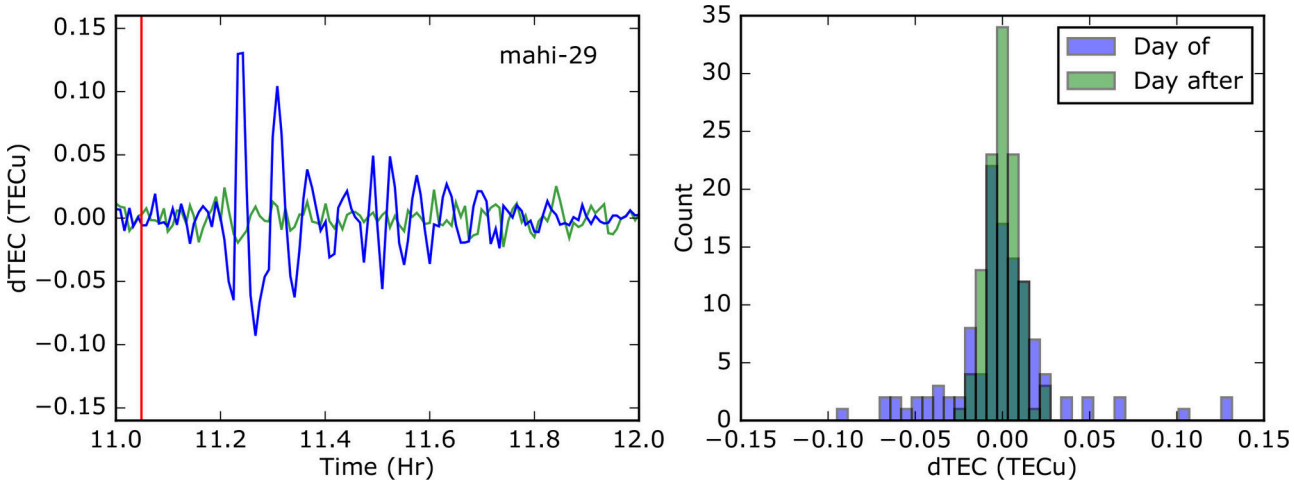

2018ja025376-t-f01-z-.eps

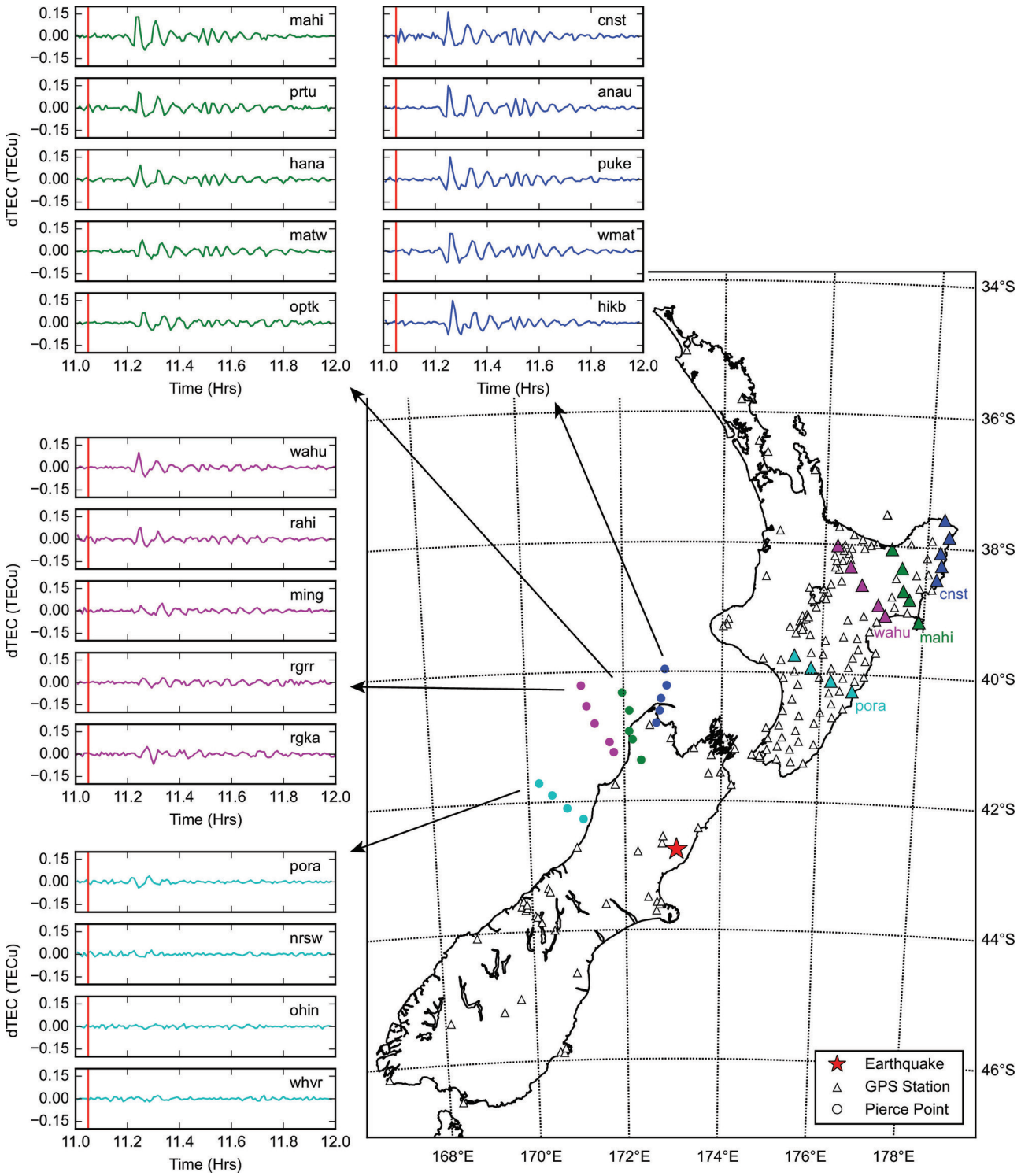

2018ja025376-t-f02-z-.eps

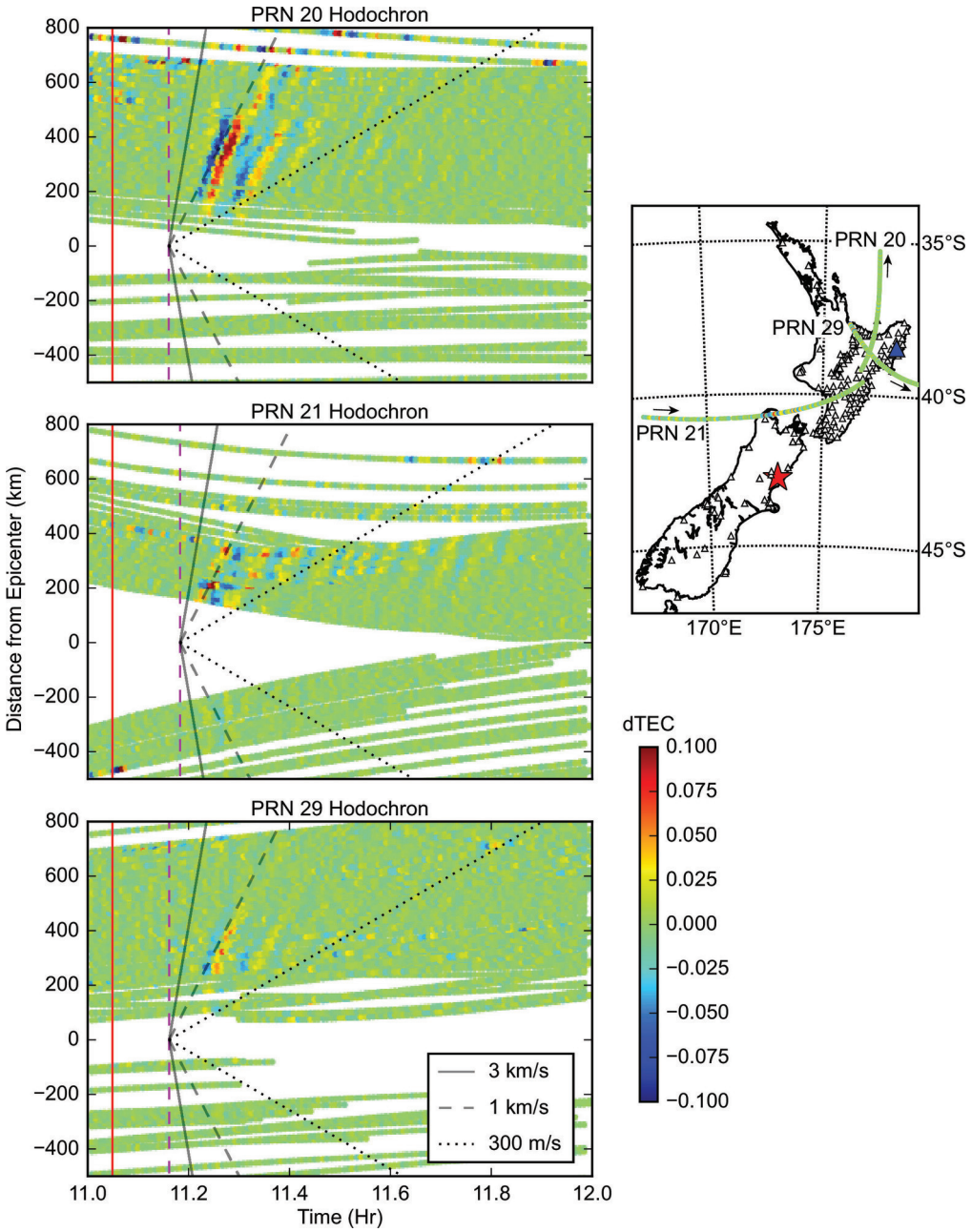

2018ja025376-t-f03-z-.eps

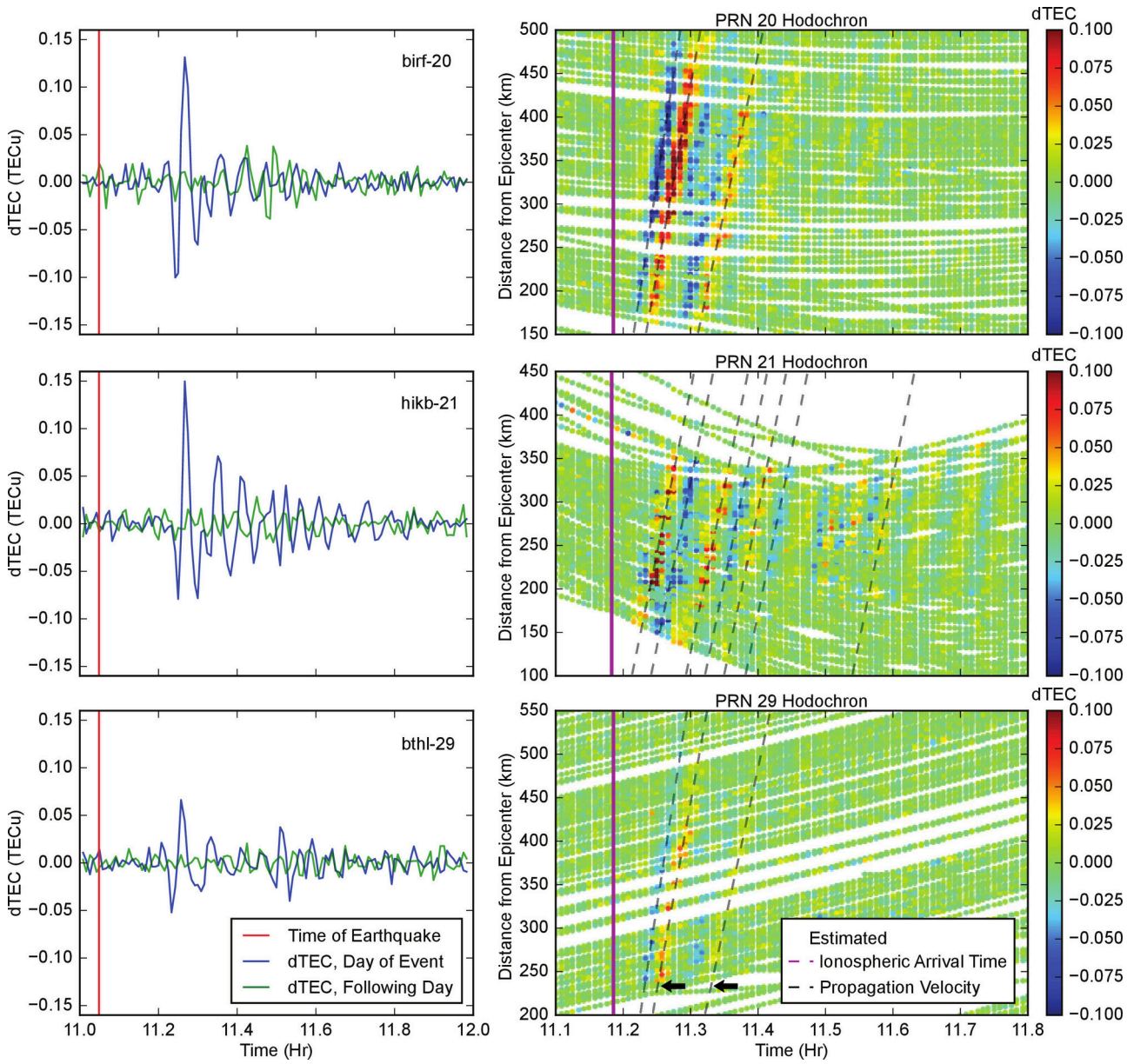

2018ja025376-t-f04-z-.eps

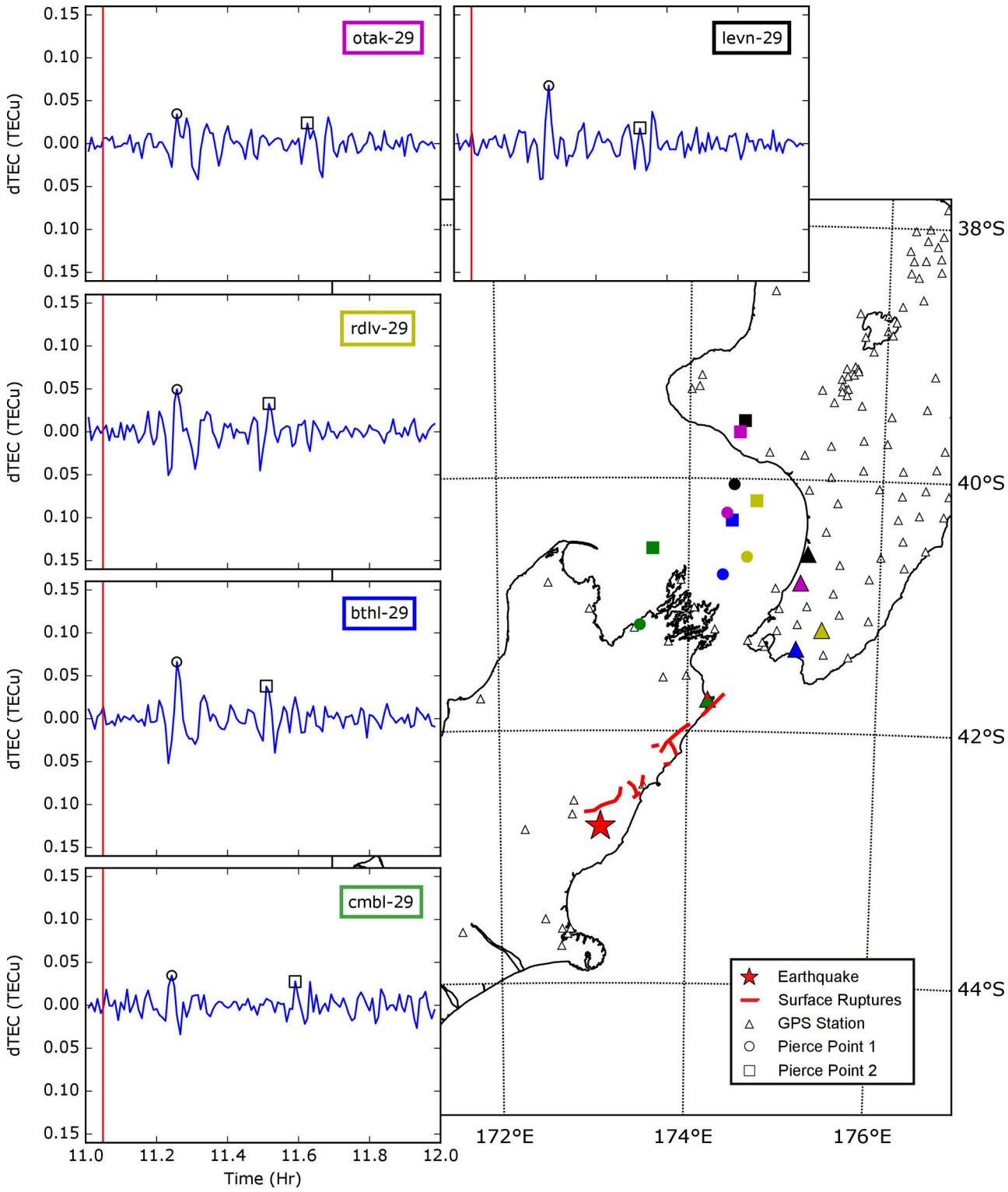

2018ja025376-t-f05-z-.eps